Simple and sustainable preparation of non-activated porous carbon from brewing waste for high-performance lithium–sulfur batteries

Alvaro Y. Tesio*[a], Juan Luis Gómez-Camer[b], Julián Morales[b], Alvaro Caballero*[b]

[a] Centro de Investigación y Desarrollo en Materiales Avanzados y Almacenamiento de Energía de Jujuy CIDMEJu (CONICET-Universidad Nacional de Jujuy), Centro de Desarrollo Tecnológico General Savio, 4612 – Palpalá, Jujuy, Argentina

[b] Departamento de Química Inorgánica, Instituto Universitario de Investigación en Química Fina y Nanoquímica (IUNAN), Campus de Rabanales, Universidad de Córdoba, 14071 Córdoba, España

*Corresponding authors:

e-mail addresses: atesio@cidmeju.unju.edu.ar (A. Y. Tesio), alvaro.caballero@uco.es (A. Caballero)

ToC

Abstract

The large development of renewable energy sources requires the parallel development of sustainable energy storage systems because of its non-continuous production. Even the most-used battery on the planet, the lithium-ion battery, is reaching its technological limit. In this reality, the lithium–sulfur battery emerges as one of the most promising technologies to face this problem. The use of biomass to produce cathodes for these batteries addresses not only the aforementioned problem, but also it reduces the carbon footprint and gives added value to something normally considered waste. Here we report the production, by simple and non-activating pyrolysis, of a carbon material using the abundant 'after-boiling waste' derived from beer brewing. After adding a high sulfur loading (70%) to this biowaste-derived carbon by the '*melt diffusion*' method, the sulfur–carbon composite was used as an effective cathode in Li–S batteries. The cathode showed excellent performance, reaching high capacity values and ultra-long cyclability at high current: 847 mAh g^{-1} (at 1C), 586 mAh g^{-1} (at 2C) and even 498 mAh g^{-1} (at 5C) after 400 cycles, drastically reducing the loss of capacity per cycle to values close to 0.01% per cycle. This work demonstrates the possibility of obtaining low-cost, highly sustainable cathodic materials for the design of advanced energy storage systems.

Keywords: lithium–sulfur batteries; waste-derived carbon; brewing process; sulfur composite

Introduction

There is no longer any legitimate doubt regarding global warming, which is a well-known fact that demands all humans to reduce the emissions released to the atmosphere, as well as the amount of waste generated on the planet. As the production of renewable energy increases, the development and continuous improvement of energy storage systems becomes necessary, mainly because all renewable energy sources (solar-derived, wind, tidal wave, etc.) are not constant. Classic batteries such as lead–acid, nickel–cadmium and lithium-ion have been, and are still, very useful;[1] however, nowadays the requirements for storing energy are much higher. Even the revolutionary lithium-ion battery, which has been on the market since 1991[2] and is still around us, is reaching its technological limit (especially when the energy requirements for the next generation of electric and hybrid electric vehicles are considered).[3]

Beyond lithium-ion batteries, there are several technologies that show promise for providing solutions to current energy storage problems.[4] Amongst them, the lithium–sulfur (Li–S) battery appears to be one of the most promising technologies, considering both its potentiality (theoretical specific capacity of 1675 mAh g^{-1} and theoretical energy density of 2600 Wh kg^{-1}) and its present state of development.[5]

In essence, a Li–S battery is formed by a sulfur cathode, a lithium anode, and an organic liquid electrolyte.[6] During discharge, the solid elemental sulfur (S_8) is reduced to soluble lithium polysulphide (Li_2S_8), producing a voltage plateau around 2.2–2.3 V. After that, a liquid–liquid single-phase reduction takes place, converting the dissolved Li_2S_8 to low-order polysulphides, increasing the viscosity and reducing the potential plateau value. Following this step, the short-chain polysulphides are reduced to lithium disulphide (Li_2S_2) and lithium sulphide (Li_2S) in a liquid–solid two-phase reduction reaction, both compounds insulating and insoluble in usual organic solvents. This reaction produces a second voltage plateau at about 1.9–2.1 V, offering

the largest battery capacity. Finally, the process ends with a rapid decrease of potential due to the solid–solid reduction from Li_2S_2 to Li_2S.[7,8]

As in any new development, there are many lines of research trying to solve the main problems of these technologies. Within them, one very extensive field is that related to the cathode problems, such as volume change, polysulphide *shuttle effect*, electric contact, conductivity, etc.[9–11] Probably the largest separation in this area is between cathodes formed by carbonaceous materials and cathodes produced without carbon (or with a low percentage of carbon). The former have the advantage of carbon's great abundance, its high conductivity and its low cost[12] and the latter, those formed by non-carbonaceous materials, have more specific advantages, related to the operation of the battery (i.e., soft structures which accommodate the volume changes, stronger interaction between sulfur and the host, and the different sulfur composites, etc.).[13] Therefore, due to the predominance of cost and availability, carbon's properties tunability – i.e. electronic conductivity, structural stability and electrochemical inertness at the operating potential – , and even historical reasons over other materials, it is that carbon cathodes are more extended used in research related to Li–S batteries.

In line with transition to renewable energy and decreasing the global carbon footprint, it is essential to keep in mind the famous 'three Rs' (recycle, reuse and reduce). Concerning that, recycling and reuse add value to various materials, previously considered as waste, that may have some other uses.[14–15] A clear example of this is the use of organic waste to produce carbon materials, used as cathodes in Li–S batteries. In recent years, an extensive bibliography on this subject has been produced; some of the most interesting and recent examples are mentioned below.[16] Kim and co-workers (2017) fabricated a highly porous carbon using waste green tea powder via carbonisation at 600 °C and a KOH activation process at 800 °C.[17] Zheng´s group (2018) described the synthesis of N and O dual-doped hierarchical porous carbon resulting from rapeseed meal. By KOH activation, they obtained an extremely high specific surface area of

2434.9 $m^2 g^{-1}$ and large total pore volume of 1.49 $cm^3 g^{-1}$. The material was tested as the cathode in Li–S batteries, with a sulfur loading of 71%.[18] Meanwhile, Ramesha and Babu (2019) used a biowaste bagasse that was converted into nitrogen-doped carbon using melamine. They found that using a ratio of carbon to melamine of 1:15 (wt/wt) can produce an excellent cathode material.[19] Pietrzak and co-workers (2020) reported a composite sulfur cathode using a hierarchical carbon obtained from waste PET bottles (through K_2CO_3 activation).[20] Practically all the carbon reported for this application has been obtained by controlled pyrolysis of the waste (or biomass), using chemical (NaOH,[21] KOH,[22,23] H_3PO_4,[24,25] $ZnCl_2$,[26,27] K_2CO_3,[28] $KHCO_3$[29]) or physical activating agents (carbon dioxide flow, steam).[30] This additional activation step increases the complexity and cost of the process, but it is necessary in these biomass-derived carbons to expand the specific surface area and pore volume. [31-33]

In beer production, the fresh wort contains a large amount of suspended solids when removed from the kettle. These solids are mainly constituted of hop leaves and Irish moss (a clarification agent). The remaining solids precipitate in variable compositions, usually named as 'hot trub'. So, this portion known as hot trub is the proteic, insoluble precipitate, with a non-defined particle size, reported from 24 to 700 μm[34] and 30 to 80 μm[35]. These particles are produced during the boiling step and must be eliminated before the fermentation process. If not, they can affect the flavour stability, or even increase the bitterness of the beer.[36] The sum of these three components (hot trub + used hops + used Irish moss) is usually called 'after-boiling waste'.

Regarding waste production, it is worth mentioning that both large factories and small craft breweries are increasing their production significantly throughout the world. Considering the volume of beverages consumed around the world, beer is the fifth most consumed, only being exceeded by tea, carbonated drinks, milk, and coffee,[37] making this an appealing industry as a source of biomass residual. Only taking Europe into account, its beer production was 400 million hectolitres in 2018, with a rough estimate of 20 kg (80% wet) of solid organic waste

per hectolitre of beer produced.[38] That means the beer brewing process provides large amounts of solid waste, which should have a final disposal that affects the environment as little as possible.[39] Today, the main use of these production wastes is animal food, which has a very low added value.[40]

It appears that, there is a small number of works where the production of carbonaceous materials derived from beer waste was reported, mainly using only the lees waste of the production. Some of them report manufacture and characterisation of the carbonaceous material or its use in a non-energy-related topic[41–45] and other applications, even reporting its use in hydrogen storage[46] or capacitors.[47]

Thus, in the present work we report, for the first time, obtaining by a simple pyrolysis process a dual-porosity carbon, derived from after-boiling waste (ABW), and its use in cathodes of Li–S batteries. This carbonaceous material, named ABW-C, was obtained without the use of chemical agents or additional activation steps and was fully morphologically, compositionally and electrochemically characterised. After the addition of a high percentage of sulfur (70%) by the melt-diffusion method, this composite was used as a sustainable cathode in Li–S batteries, showing excellent performance reaching high capacities and ultra-long cyclability at high cycling rates.

Experimental Section

Preparation of 'After-Boiling Waste'-derived Carbon (ABW-C)

'After-boiling waste'-derived carbon (ABW-C) was produced using a sub-product of beer manufacturing. In a typical fabrication, the after-boiling waste that come directly from the factory was dried at 110 ºC overnight. Then, the dried material was heated from 110 °C to 900

°C, using a heating ramp of 15 ºC min^{-1}, where it was held for 60 min for carbonisation. Both processes were carried out under a nitrogen atmosphere, with a flow rate of 50 mL min^{-1}. Once obtained, the carbonised product was milled at 100 rpm for 1 h using a ball mill (Retsch PM100, Retsch GmbH, Haan, Germany). No further activation or washing was needed.

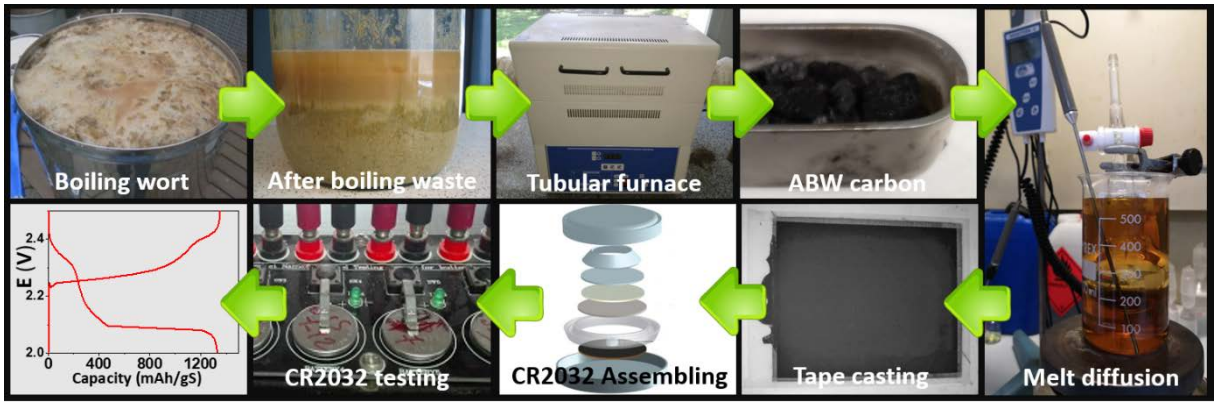

Scheme 1. Scheme of battery cathode fabrication from beer production waste and battery testing.

Synthesis of Carbon–Sulfur Composite (ABW-C@S)

To prepare the composite, sulfur was added to ABW-C by using the melt diffusion method.[48] Both materials were mixed inside a glove box in Ar atmosphere (M-Braun 150 model, under 1 ppm water and oxygen conditions) in a weight ratio of 70:30 (S : ABW-C), and then taken out in a closed round-bottom flask. The closed flask was heated at 155 °C in a glycerine bath for 6 h. The sulfur content was confirmed by thermo gravimetric analysis (TGA); it was 70%.

Sample Characterisation

X-ray diffraction (XRD) patterns were recorded with a Bruker D8 Discover X-ray diffractometer using monochromatic Cu Kα radiation. The scanning conditions for structural analysis were 5–80° (2Θ), a 0.015° step size, and 0.1 s per step. The scanning electron microscope (SEM) analysis of the samples was performed by using a JEOL JSM 6300 equipped

with microanalysis system Inca Energy 250. The carbon content in the carbon material and sulfur content in the composite were determined by thermogravimetric analysis using a Mettler Toledo TGA/DSC with the following parameters: carbon—heating rate of 5 °C min^{-1} from 25 to 900 °C under oxygen atmosphere; composite—heating rate of 5 °C min^{-1} from 25 to 600 °C under nitrogen atmosphere. The textural properties were determined by a Micromeritics ASAP 2020 system using nitrogen as adsorbent and Brunauer–Emmett–Teller (BET) method. Pore size distribution was calculated by the density functional theory (DFT) method.

Cell Assembly and Electrochemical Characterisation

Slurry for electrodes was prepared in a weight proportion of 85:10:5 of ABW-C@S composite to PVDF binder (Sovay) to carbon Super P (Timcal), respectively. These mixtures were treated with 1-methyl- 2-pyrrolidinone (Sigma-Aldrich) to obtain a slurry that was deposited on gas diffusion layer (GDL) foil by using the tape casting technique. GDL carbon cloth has proven to be an effective current collector in cathodes of Li–S cells.[49] The sulfur loading was around 1 mg cm^{-2} for the cathode. The electrolyte was LiTFSI 1M (Sigma Aldrich) and $LiNO_3$ 0.4 M (Sigma Aldrich) in 1,3-dioxolane (DOL, Sigma Aldrich) and 1,2-dimethoxyethane (DME, Sigma Aldrich) (1:1 v/v), soaked in a polyethylene membrane (Celgard 2400), with a porosity of 39% and a thickness of 25 μm, which was used as anode–cathode separator. The electrolyte amount was around 20 μL. The electrolyte-to-sulfur ratio in the studied cells was 20 uL/mgS. Li metal foil was utilised as the counter and reference electrodes. Cyclic voltammetry (CV) measurements were recorded at a scan rate of 0.1 mV s^{-1} by using a Solartron 1286. Galvanostatic charge–discharge (GCD) experiments were performed on an Arbin BT2000 potentiostat–galvanostat system, using CR2032 coin cells. The cells were assembled inside an Ar-filled glove box. The specific capacity values were calculated based on the sulfur loading in the electrode.

Results and Discussion

In order to use any carbon as a material host in Li–S battery cathodes, the textural properties of this carbon must be analysed in detail. Fig. 1a shows the nitrogen adsorption–desorption isotherm of the carbon derived from brewing waste (ABW-C). The shape of the curve can be classified between two kinds of isotherms in the Brunauer-Deming-Deming-Teller (BDDT) classification. Type I, typical of micropore systems and type IV, evident at high relative pressures, characteristic of mesoporous solids. The presence of a small hysteresis loop in the desorption branch, type H4 in the IUPAC classification, is indicative of a narrow slit-like mesoporous system. Therefore, the isotherm reveals the micro- and mesopore structure of the ABW-C, which has already been described for other carbons derived from natural organic products.[50,51] The pore size distribution calculated by DFT method, Fig. 1b, confirms the dual micro- and mesoporous structure of the ABW-C. From this isotherm, total pore volume of 0.277 $cm^3\ g^{-1}$, with a micropore volume of 0.141 $cm^3\ g^{-1}$, can be calculated (approx. 50% microporosity). Related to the pore volume (Fig. 1b), it becomes plain that there is a binomial distribution of the pore diameter, with maxima centred at pore diameters of 0.8 and 2 nm, consistent with the presence of micropores and small mesopores, respectively. In the case of the micropores, diameters are distributed between 0.6 and 1.0 nm, and the small mesopores start from a pore diameter of 1.8 nm, with the mentioned peak at 2.0 nm, but including a gradual decrease of pore volume as the diameter of the same increases. This small size pore structure is reported to potentially limit the diffusion of soluble polysulphides effectively through physical adsorption, thus decreasing the 'polysulphide shuttle' and enhancing the sulfur utilisation rate.[52] BET surface analysis shows a total surface area of 414 $m^2\ g^{-1}$. Meanwhile the t-plot analysis indicates that a significant fraction of the carbon surface area (288 $m^2\ g^{-1}$) is associated with the presence of micropores. The high surface area of ABW-C favours the sulfur

distribution in the carbon framework, the molten sulfur thus can easily permeate into the ABW-C by capillary force, the specific surface area and pore volume of the resulting ABW-C@S composite then being significantly reduced (5 m^2 g^{-1} and 0.035 cm^3 g^{-1}, respectively). According to this textural analysis and in comparison with carbons of similar nature,[25] carbon derived from brewing waste possesses suitable textural properties for application in Li–S batteries: a high surface area for sulfur deposition and an interconnected micro- and mesoporous system that will be able to trap polysulphides and hinder their solubility in the electrolyte.

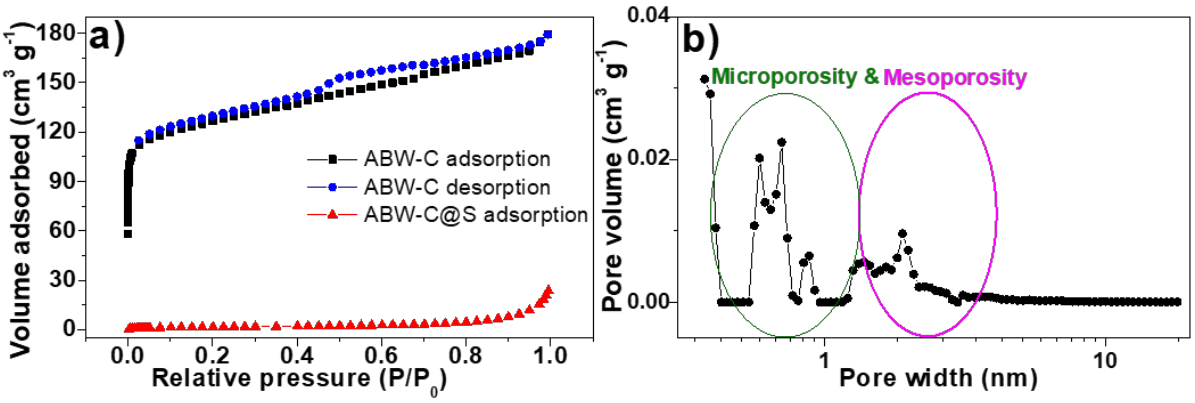

Figure 1. a) Nitrogen adsorption–desorption isotherms for ABW-C and ABW-C@S samples; b) Pore size distribution of the ABW-C obtained by DFT method (logarithmic scale)

TG analyses were performed on the ABW-C material in oxygen atmosphere in order to know its carbon content, and on the ABW-C@S composite in nitrogen atmosphere to know its sulfur content (Fig. 2a). In the first case, a carbon percentage of 88% was obtained. This is a value that confirms a material with a high carbon content, a strictly necessary condition for suitable carbon materials from biomass or industrial waste. Likewise, this means that the ash content was low and, consequently, the non-electroactive impurity content was relatively low. The ash content is slightly higher than that reported for other biomass-derived coals, where acid activating agents reduced part of these mineral substances[53]. In the second case, the sulfur percentage obtained for the composite was 70%, the exact amount of sulfur that was utilised

during the melt diffusion technique to impregnate the ABW-C, indicating that no sulfur was lost during the synthesis of ABW-C@S composite.

The XRD pattern of the ABW-C (Fig. 2b) shows the expected two broad peaks of low intensity, with the peaks centred at 25 and 44º coming from to the crystallographic planes of graphite (002) and (100), respectively. The weak peak intensity with respect to the background and the huge peak width are typical of highly disordered carbons.[30] It is important to note that no other crystalline phases were found in the samples, and neither peak was observed at 2θ at angles below 10°, which indicates no presence of order at the mesopore level.[54] The XRD pattern of ABW-C@S composite showed the characteristic sharp and well-defined peaks of the orthorhombic sulfur polymorph (PDF No. 85-0799), showing the presence of crystalline sulfur. This crystalline phase of sulfur is frequently described in sulfur-carbon composites obtained using the melt diffusion method [18,21,23,24]. Although the absence of any type of these peaks has also been reported, due to the lack of crystallinity of the sulfur in its composites [55, 56] o that sulfur exists as a highly dispersed state inside the pores of carbon [57, 58].

Structural analysis of ABW-C and ABW-C@S composite was conducted by Raman spectroscopy, as shown in Fig. 2c. There were two partially overlapped bands at around 1347 and 1597 cm^{-1} for the ABW-C. As we found previously in the XRD patterns, the Raman spectrum showed a typical profile of poorly graphitised carbon. But in this experiment, we could also observe the well-known D-band and G-band, which indicates good electrical conductivity.[59] Generally, the D-band indicates disordered graphitic carbon, whilst the G-band is ascribed to the crystalline graphite structure.[60] The relative intensity ratio I_D/I_G is proportional to the level of defects in carbon materials. The value of I_D/I_G for ABW-C was 1.00, indicating a high electronic conductivity.[59] The I_D/I_G ratio remains constant (decreasing only 0.01) after impregnation with 70 wt % sulfur, implying that no additional lattice defects emerged.[60] Crystalline sulfur exhibits the characteristic sharp peaks, amongst them the peaks

between 150 and 270 cm^{-1} attributed to the bending mode and the peaks between 400 and 550 cm^{-1} attributed to the stretching mode, both of elemental α-S_8.[61] It should be noted that the presence of the signals due to S would be justified when a slight excess of sulfur is present in the composite. This fact indicates that not all sulfur is confined in the pores of the carbon matrix but that part of this sulfur is deposited on the surface.[62]

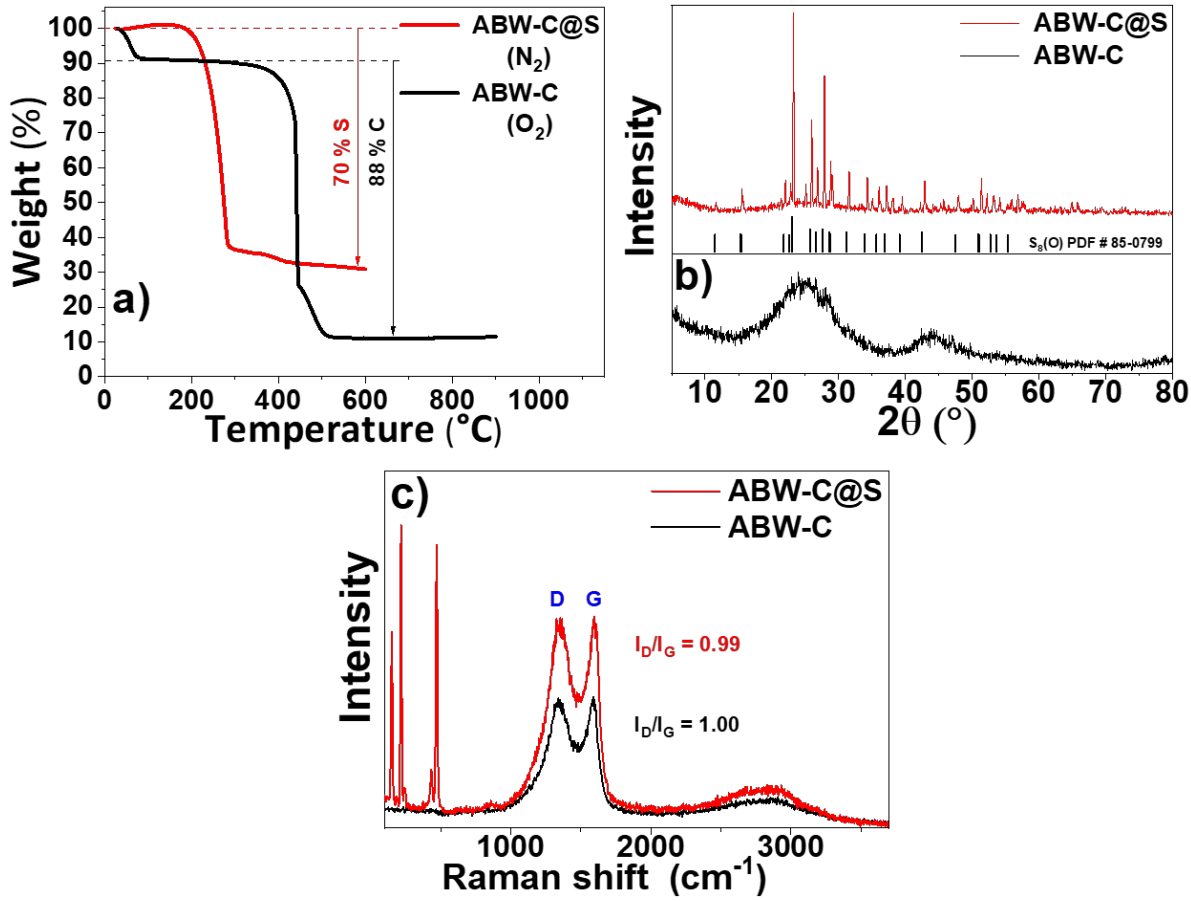

Figure 2. ABW-C and ABW-C@S composite analyses: a) TG curves; b) XRD patterns; and c) Raman spectra.

It is well known that the SEM technique possesses limitations in the study of (micro- and meso-) porous solids, as the micrographs can only provide a partial image of the external particle surface. Nevertheless, SEM can still supply information on the size and shape of the particles. SEM images Fig. 3a and 3b depict heterogeneous micrometric particles of ABW-C and ABW-C@S composite. The particles differ only in the fact that the particle in Fig. 3b was impregnated

with sulfur. Note that no size or morphology modification is observed after the sulfur loading. Fig. 3c and 3d show a typical particle of ABW-C@S composite together with its elemental sulfur maps. By observation of these images, it is confirmed that there are no sulfur agglomerates on the ABW-C@S composite surface. So, the elemental sulfur was homogeneously distributed inside the framework of the porous carbon, which implies good confinement of it.[63,64] All of these results confirm that most of the sulfur loading occupies the cavities in the dual pore system, a conclusion that is in good agreement with the drastic reduction in surface area and pore volume observed in the ABW-C@S composite compared to ABW-C.

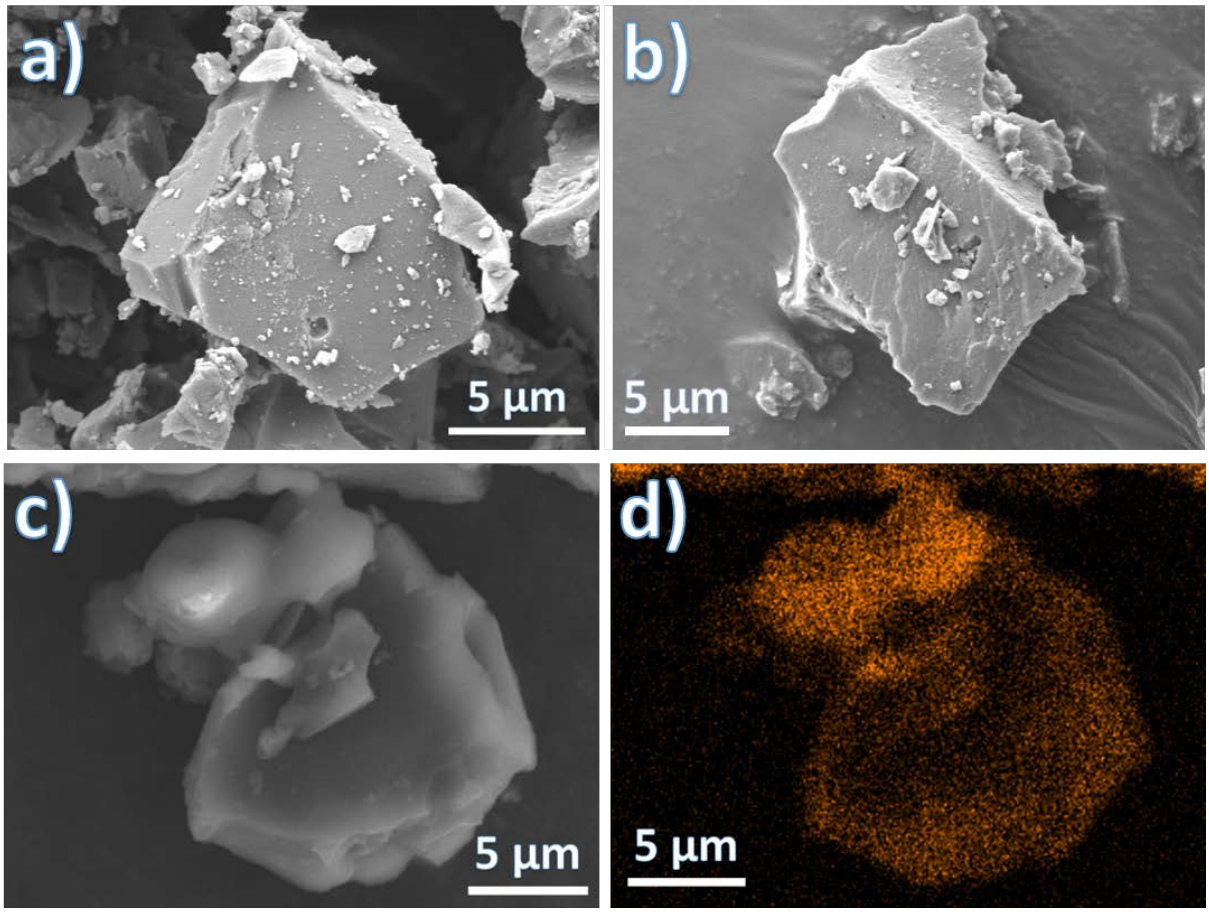

Figure 3. SEM images of a) ABW-C and b) ABW-C@S composite. SEM-EDS images of c) ABW-C@S composite and d) the corresponding elemental sulfur map

The electrochemical properties of CR2032 coin cells, assembled with lithium foil as the anode and ABW-C@S composite as the cathode, were then studied. Fig. 4a shows the cyclic voltammetry (CV) profiles of the ABW-C@S composite obtained at a scanning rate of 0.1 mV s^{-1} between 1.7 and 2.9 V. The multistep reduction of sulfur, as in the case of Li–S batteries, is a widely studied process.[65] The first step is generally attributed to the opening of the S_8 ring, resulting in the formation of long-chain polysulphides (Li_2S_x, $4 \leq x \leq 8$). The second step is associated with a further reduction of these polysulphides to short-chain polysulphides (Li_2S_2 and Li_2S). The slowness of these reactions causes a polarisation and a significant overlapping of both reactions, resulting in the appearance of an asymmetric peak. For the ABW-C@S cathode, just one reduction peak centred at 2 V is observed and must be assigned to the multistep reduction of sulfur with overlapped signals. CV profiles of similar characteristics have been previously reported for other C-S composites[66, 67]. Additionally, this overlap may also be due to the low dielectric constant of the mixed solvent used (low donor numbers: DOL ~18 and DME ~24 kcal/mol). Here, the solvents cannot suitably solvate the S_8^{2-} anion, so its production is not energetically favoured, shifting cathodic potentials to higher values than other solvents and producing a multiple-electron transfer at the same potential, which is observed as one single peak or two blended peaks, depending on several factors.[68]

The oxidation process in the Li–S battery occurs in two stages.[7,65,69] In the present case, the anodic scan shows an asymmetric wide peak centred at 2.65 V, attributed to the reverse reactions of those produced during the reduction. Similar to what occurred in the cathodic scan, the low dielectric constant of the mixed solvent that was used, combined with the low speed of these reactions, caused overlapping of both reactions, resulting in one asymmetric peak. The high reversibility of the whole process is evident, because when cycling the cell, the shape of the curves does not undergo any significant change.[68]

Galvanostatic charge and discharge curves were recorded between 1.8 and 2.7 V at different rates (1C = 1675 mA g^{-1}) and are shown in Fig. 4b. During the discharge, two processes were observed: one quasi-voltage plateau from 2.3 to 2.4 V and one well-defined voltage plateau between 2.0 and 2.1 V (depending on the current), consistent with the peak shape described for the CV curve. In the charging curve, two well-defined voltage plateaus are detected at 2.2 and 2.4 V, coherent with the one asymmetric oxidation peak observed in the CV curve. Regarding the discharge curves, all display two typical plateaus related to the mechanism of the electro-chemical Li–S reduction.[7,59,69] Note that the low voltage oxidation plateau (2.2 V) was strongly polarised. This phenomenon is frequently observed in carbon-based sulfur composite cathodes.[70,71] Moreover, the small differences between the voltages of these two plateaus are consistent with the observation of only one asymmetric oxidation peak in the CV curve.

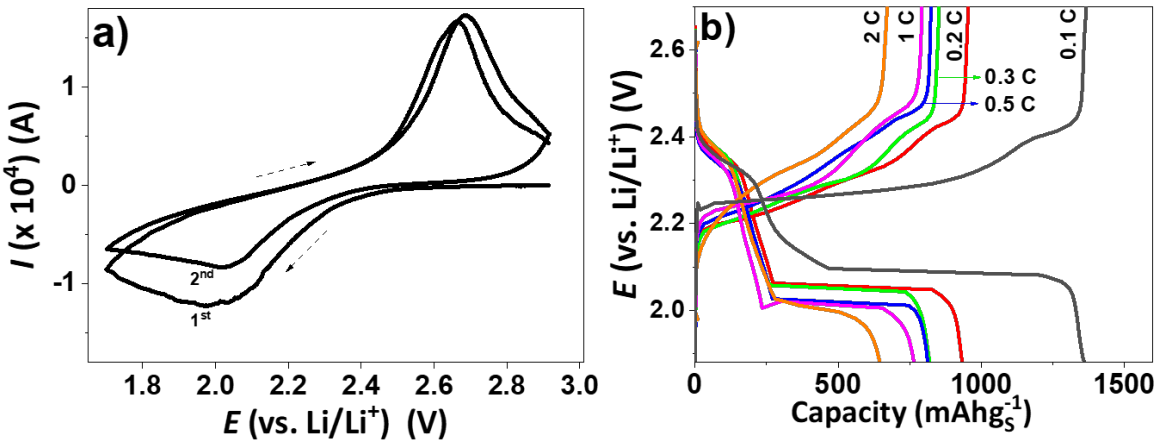

Figure 4. Li–S battery using an ABW-C@S composite cathode. a) CV profile at a scan rate of 0.1mV s^{-1} and b) discharge–charge profiles at different C rates

As expected, the discharge capacity values decrease as the current density increases. However, outstanding behaviour was found even when cycling at high current densities, such as 1C and 2C (Fig. 5). Fig. 5a shows the cycling performance of a Li–S battery using an ABW-C@S composite cathode at a current density of 1C. In order to facilitate data analysis, we separated Fig. 5a into three different zones: I, II and III. In zone I, which includes the first 25 cycles of

the battery, the 'electrochemical stabilisation' of the battery is produced, in which irreversible reactions take place and cause an abrupt potential drop, typical for this kind of battery.[70,71] Here, in zone I, the battery reaches a high capacity value of 1361 mAh g^{-1} in the 3rd cycle. This value starts to decrease until the 25th cycle, when the battery achieves its stabilisation. During zone I, the capacity loss is close to 10 mAh g^{-1} per cycle (0.73% per cycle). Zone II is characterised by a full stabilisation of the battery, cycling 175 times with a capacity loss of only 0.29 mAh g^{-1} per cycle (0.025% per cycle), at an average capacity value of 1100 mAh g^{-1}. Finally, in zone III the battery starts to show a progressive decay, possibly due to mechanical reasons (loss of electrical connection at the cathode, electrolyte drying, etc.). Whilst it is true that the battery at this point does not have the same performance as in zone II, it is also true that it still has some useful energy, accomplishing 450 cycles while maintaining a capacity value greater than 800 mAh g^{-1} and with a capacity loss of 2.5 mAh g^{-1} per cycle (0.23% per cycle), in this zone. If all the cycling of the Li-S cell is analysed, the average capacity loss is 1.24 mAh g^{-1} per cycle (0.09% per cycle). In addition, the coulombic efficiency of the cell is represented on the right axis. Values close to 95% can be observed, whilst for the remaining cycling rates these values are close to 100%.

Taking consideration of the excellent behaviour of the ABW-C@S cathodic composite at 1C rate, this was tested at even higher current densities. The results are shown in Fig. 5b. At a current density of 2C, the battery was tested more than 600 cycles and ended the cycling with capacity values greater than 450 mAh g^{-1} and accumulated a whole capacity loss of 2.5 mAh g^{-1} per cycle (0.12% per cycle). The battery cycled at a current density of 5C accomplished 950 cycles, culminating with a capacity value greater than 270 mAh g^{-1}. Note that this battery ended its stabilisation phase with a capacity value of 500 mAh g^{-1} after 400 cycles. The total capacity loss was 1.15 mAh g^{-1} per cycle (0.01% per cycle). More strikingly, after more than 1000 cycles at 5C, the Li/LiTFSI-$LiNO_3$-DOL:DME/ABW-C@S cell was still working, providing 100%

coulombic efficiency after activation cycles and exhibiting remarkable cycling stability. In both cases, the three zones could be delimited in the same way that in the 1C test: Zone 1 (25th first cycles), Zone 2 (between 25th and 200th cycles) and Zone 3 (from 200th cycle to the end). For the 2C battery, due to the shape of the capacity decrease, maybe the zone 3 could be extended until the 300th cycle. It is noteworthy that in this third zone, the loss of capacity per cycle is even less for tests 2C (0.07% per cycle) and 5C (0.11% per cycle) than that calculated for 1C (0.23%).

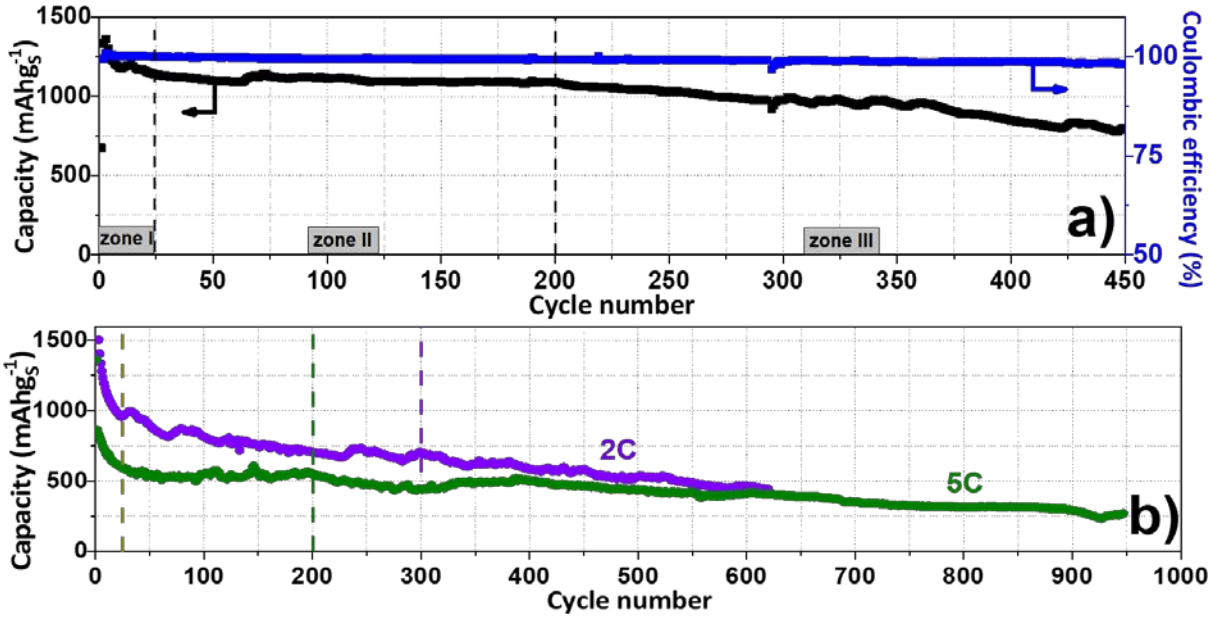

Figure 5. Long-term cycling performance of ABW-C@S composite in Li–S cell at high rates: a) 1C; b) 2C and 5C

Thus, the remarkable cycling properties of our carbon require an explanation based on arguments related to its textural properties: The interconnected hierarchical pore system, micropores and mesopores, is able to trap the polysulphides and buffer the expansion and contraction of sulfur nanoparticles during the reversible reaction with Li. In relevant studies related to the field of bio-mass (waste)-derived materials used as cathodes in Li–S batteries mentioned above, it has been found that: (i) Kim and co-workers obtained a specific capacity for the first discharge of 712 mAh g^{-1}, cycling 50 times and reaching a capacity value of 500

mAh g^{-1}.[17] (ii) Zheng´s groups obtained a capacity value of 1259 mAh g^{-1} for the first discharge and maintained a capacity value of 512 mAh g^{-1} after 200 cycles.[18] (iii) Ramesha and Babu achieved a capacity value of 1169 mAh g^{-1} at 0.2C and retained 898 mAh g^{-1} after 200 cycles, and 454 mAh g^{-1} at 4C, for the same number of cycles.[19] Finally, (iv) Pietrzak and co-workers obtained a specific discharge capacity of 829 mAh g^{-1} at 0.05C and accomplished 50 cycles with a capacity value of 712mAh g^{-1}.[20] In comparison with these important studies and even with very relevant recent reports of non-biomass-carbon cathodes, such as that published by Carbone and co-workers,[72] it is remarkable that in the present work we have obtained higher capacity values, lower loss capacity values in cycling, and ultra-long cyclability even at high discharge rates. These remarkable improvements have been achieved using a high sulfur content (70%) in the composite and a high percentage of active composite (85%) in the positive electrode. Note that no activation or treatment has been performed on the composite material obtained. Therefore, after-boiling waste, a non-economically valued biowaste derived from brewing, has been shown to be an ideal carbon precursor for obtaining a porous carbon as an effective sulfur host for preparing high-performance cathodes for Li–S batteries. However, for practical applications it is necessary that the areal loading of sulfur must be increased, with values starting from 2 mg cm^{-2} [73], or even above 6 mg cm^{-2} [9]. Accordingly, further studies aiming to increase the areal sulfur loading of ABW-C@S electrodes are certainly required.

Conclusions

The boom in the production of biomass-derived materials has been generated because of the need to diminish pollution in the world through recycling and reuse. These result in decreasing the carbon footprint on the planet and many times, in parallel, reducing production costs. In the case of carbon materials derived from biomass, applied to energy storage, it is a real success because of its low cost and easy production. So, for Li–S batteries, these materials are attractive because they represent a suitable and cheap matrix in which the sulfur reactions can take place.

Carbon derived from brewing waste, without any activation process, has demonstrated suitable textural properties for the preparation of high-sulfur-content composites to use as effective cathodes in Li–S cells. Its high surface area, combined with its interconnected micro- and mesoporous system, raises its performance, in both capacity values and cyclability, even at high current densities. Therefore, this work demonstrates the possibility of revaluing the brewing waste by transforming it into a porous carbon, using a simple process without activation stages, with promising performance in a sustainable cathode in ultra-high-cyclability Li–S batteries.

Acknowledgements

This research was funded by Ministerio de Economía y Competitividad (Project MAT2017-87541-R) and Junta de Andalucía (Group FQM-175). AYT was a CONICET Research Fellow. We would like to thank MSc. Silvia Cassinera and Dr. Gustavo Scalone, from the brewery Graslei, for providing the 'after-boiling waste' from their production.

References

[1] C.-X. Zu, H. Li, *Energy Environ. Sci.* **2011**, *4*, 2614–2624.

[2] J. B. Goodenough, K. S. Park, *J. Am. Chem. Soc.* **2013**, *135*, 1167–1176.

[3] A. Fotouhi, D. J. Auger, K. Propp, S. Longo, M. Wild, *Renew. Sust. Energ. Rev.* **2016**, *56*, 1008–1021.

[4] H. Zhang, X. Li, H. Zhang, *Li–S and Li–O2 Batteries with High Specific Energy*, Springer Singapore, **2017**.

[5] T. Li, X. Bai, U. Gulzar, Y. J. Bai, C. Capiglia, W. Deng, X. Zhou, Z. Liu, Z. Feng, R. Proietti Zaccaria, *Adv. Funct. Mater.* **2019**, *29*, 1901730–1901786.

[6] A. Manthiram, Y. Fu, A-S. Su, *Accounts. Chem. Res.* **2013**, *46*, 1125–1134.

[7] D. Zheng, D. Liu, J. B. Harris, T. Ding, J. Si, S. Andrew, D. Qu, X. Q. Yang, D. Qu, *ACS Appl. Mater. Inter.* **2017**, *9*, 4326–4332.

[8] S. S. Zhang, *J. Power Sources* **2013**, *231*, 153–162.

[9] H-J. Peng, J-Q. Huang, X-B. Cheng, Q. Zhang, *Adv. Energy Mater.* **2017**, *7*, 1700260–1700314.

[10] W. Kang, N. Deng, J. Ju, Q. Li, D. Wu, X. Ma, L. Li, M. Naebe, B. Cheng, *Nanoscale* **2016**, *8*, 16541–16588.

[11] C. Dong, W. Gao, B. Jin, Q. Jiang, *iScience* **2018**, *6*, 151–198.

[12] S. Li, B. Jin, X. Zhai, H. Li, Q. Jiang, *ChemistrySelect* **2018**, *3*, 2245–2260.

[13] A. N. Arias, A. Y. Tesio, V. Flexer, *J. Electrochem. Soc.* **2018**, *165*, 6119–6135.

[14] J. Sherwood, *Bioresour. Technol.* **2020**, *300*, 122755-122762.

[15] C. Liedel, *ChemSusChem* **2020**, *13*, 2110-2141.

[16] H. Yuan, T. Liu, Y. Liu, J. Nai, Y. Wang, W. Zhang, X. Tao, *Chem. Sci.* **2019**, *10*, 7484–7495.

[17] S.-D. Seo, C. Choi, B.-K. Kim, D.-W. Kim, *Ceram. Int.* **2017**, *43*, 2836–2841.

[18] L. Xia, Z. Song, L. Zhou, D. Lin, Q. Zheng, *J. Solid State Chem.* **2019**, *270*, 500–508.

[19] D. B. Babu, K. Ramesha, *Carbon* **2019**, *144*, 582–590.

[20] P. Półrolniczak, D. Kasprzak, J. Kaźmierczak-Raźna, M. Walkowiak, P. Nowicki, R. Pietrzak, *Synthetic Met.* **2020**, *261*, 116305.

[21] M. Yu, R. Li, Y. Tong, Y. Li, C. Li, J.-D. Hong, G. Shi, *J. Mater. Chem. A* **2015**, *3*, 9609–9615.

[22] J. Wang, S. Kaskel, *J. Mater. Chem.* **2012**, *22*, 23710–23725.

[23] X. Chen, G. Du, M. Zhang, A. Kalam, Q. Su, S. Ding, B. Xu, *J. Electroanal. Chem.* **2019**, *848*, 113316–113322.

[24] J. Ren, Y. Zhou, H. Wu, F. Xie, C. Xu, D. Lin, *J. Energy Chem.* **2018,** *30*, 121–131.

[25] C. Hernández-Rentero, R. Córdoba, N. Moreno, A. Caballero, J. Morales, M. Olivares-Marín, V. Gómez-Serrano, *Nano Res.* **2017**, *11*, 89–100.

[26] A. Benítez, M. Gonzalez-Tejero, A. Caballero, J. Morales, *Materials* **2018**, *11*, 1428–1443.

[27] D-L. Vu, J-S. Seo, H-Y. Lee, J.-W. Lee, *RSC Adv.* **2017**, *7*, 4144–4151.

[28] T-T. Mai, D-L. Vu, D-C. Huynh, N-L. Wu, A-T. Le, *J. Sci.: Adv. Mater. Devices* **2019**, *4*, 223–229.

[29] X.-L. You, L.-J. Liu, M.-Y. Zhang, M. D. Walle, Y. Li, Y.-N. Liu, *Mater. Lett.* **2018**, *217*, 167–170.

[30] N. Moreno, A. Caballero, L. Hernán, J. Morales, *Carbon* **2014**, *70*, 241–248.

[31] Q. Zhu, H. Deng, Q. Su, G. Du, Y. Yu, S. Ma, Bi. Xu, *Electrochim. Acta* **2019**, *293*, 19-24.

[32] S. Zhang, M. Zheng, Z. Lin, N. Li, Y. Liu, B. Zhao, H. Pang, J. Cao, P. He, Y. Shi, *J. Mater. Chem. A* **2014**, *38*, 15889-15896.

[33] Z. Wang, X. Zhang, X. Liu, Y. Zhang, W. Zhao, Y. Li, C. Qin, Z. Bakenov, *J. Colloid Interface Sci.* **2020**, *569*, 22-33.

[34] M. Jakubowski, A. Antonowicz, M. Janowicz, M. Sterczyńska, J. Piepiórka-Stepuk, A. Poreda, *J. Food Eng.* **2016**, *173*, 34–41.

[35] Á. Varga, E. Márki, *J. Food Process Eng.* **2019**, *42*, 13200-13205.

[36] D. O. Schisler, J. J. Ruocco, M. S. Mabee, J. Am. Soc. Brew. Chem. **2018**, *40*, 57–61.

[37] L. Fillaudeau, P. Blanpain-Avet, G. Daufin, *J. Clean. Prod.* **2006**, *14*, 463–471.

[38] The Brewers of Europe, *European Beer Trends, Statistics Report*, **2019**.

[39] R. d. S. M. Thiago, P. M. d. M. Pedro, F. C. S. Eliana, *J. Brew. Distill.* **2014**, *5*, 1–9.

[40] S. I. Mussatto, G. Dragone, I. C. Roberto, *J. Cereal. Sci.* **2006**, *43*, 1–14.

[41] H. Wakizaka, H. Miyake, Y. Kawahara, *Sustain. Mater. Technol.* **2016**, *8*, 1–4.

[42] W. Hao, N. Keshavarzi, A. Branger, L. Bergström, N. Hedin, *Carbon* **2014**, *78*, 521–531.

[43] J. Hayashi, A. Kubo, A. Furukawa, K. Muroyama, *Kagaku Kogaku Ronbunshu* **2000**, *26*, 293–297.

[44] H-H. Lee, Y. Hirano, S. Matsumoto, N. Murayama, J. Shibata, *Resources Processing* **2007**, *54*, 19–24.

[45] H. Wakisaka, H. Miyake, Y. Kawahara, *Tanso* **2005**, *218*, 192–196.

[46] M. S. Balathanigaimani, M. B. Haider, D. Jha, R. Kumar, S. J. Lee, W. G. Shim, H. K. Shon, S. C. Kim, H. Moon, *J. Nanosci. Nanotechnol.* **2018**, *18*, 2196–2199.

[47] S. G. Lee, K. H. Park, W. G. Shim, M. S. Balathanigaimani, H. Moon, *J. Ind. Eng. Chem.* **2011**, *17*, 450–454.

[48] X. Ji, K. T. Lee, L. F. Nazar, *Nat. Mater.* **2009**, *8*, 500–506.

[49] A. Benítez, A. Caballero, E. Rodríguez-Castellón, J. Morales, J. Hassoun, *ChemistrySelect* **2018**, *3*, 10371–10377.

[50] K. Wang, N. Zhao, S. Lei, R. Yan, X. Tian, J. Wang, Y. Song, D. Xu, Q. Guo, L. Liu, *Electrochim. Acta* **2015**, *166*, 1–11.

[51] Y. Zhao, L. Wang, L. Huang, M. Y. Maximov, M. Jin, Y. Zhang, X. Wang, G. Zhou, *Nanomaterials* **2017**, *7*, 402–411.

[52] X. Yang, Y. Yu, N. Yan, H. Zhang, X. Li, H. Zhang, *J. Mater. Chem. A* **2016**, *4*, 5965–5972.

[53] M. Ahmedna, W. E Marshall, R. M. Rao, *Bioresour. Technol.* **2000**, *71*, 103-112

[54] B. Wang, T. P. Ang, A. Borgna, *Micropor. Mesopor. Mat.* **2012**, *158*, 99–107.

[55] H. S. Ryu, J. W. Park, J. Park, J-P. Ahn, K-W. Kim, J-H. Ahn, T-H. Nam, G. Wang, H-J. Ahn, *J. Mater. Chem. A* **2013**, *1*, 1573-1578.

[56] Z. Chen, X-L. Du, J-B. He, F. Li, Y. Wang, Y-L. Li, B. Li, S. Xin, *ACS Appl. Mater. Interfaces* **2017**, *9*, 33855-33862.

[57] B. Zhang, X. Qin, G. R. Lia , X. P. Gao, *Energy Environ. Sci.*, **2010**, *3*, 1531-1537.

[58] R. Elazari, G. Salitra, A. Garsuch, A. Panchenko, D. Aurbach, *Adv. Mater.* **2011**, *23*, 5641–5644.

[59] Z. Li, L. Yuan, Z. Yi, Y. Sun, Y. Liu, Y. Jiang, Y. Shen, Y. Xin, Z. Zhang, Y. Huang, *Adv. Energy Mater.* **2014**, *4*, 1301473.

[60] X. Tao, J. Zhang, Y. Xia, H. Huang, J. Du, H. Xiao, W. Zhang, Y. Gan, *J. Mater. Chem. A*, **2014**, *2*, 2290–2296.

[61] R. Steudel, B. Eckert, *Elemental Sulfur and Sulfur-Rich Compounds* (Ed. R. Steudel), Springer, **2003,** vol. 230, pp. 1–80.

[62] G. Zheng, Q. Zhang, J. J. Cha, Y. Yang, W. Li, Z. W. Seh, Y. Cui, *Nano Lett.* **2013**, *13*, 1265–1270.

[63] A. Rosenman, R. Elazari, G. Salitra, D. Aurbach, A. Garsuch, *J. Electrochem. Soc.* **2014**, *161*, A657–A662.

[64] N. Moreno, A. Caballero, L. Hernan, J. Morales, J. Canales-Vazquez, *Phys. Chem. Chem. Phys.* **2014**, *16*, 17332–17340.

[65] M. K. Song, E. J. Cairns, Y. Zhang, *Nanoscale* **2013**, *5*, 2186–2204.

[66] P. Półrolniczak, P. Nowicki, K. Wasiński, R. Pietrzak, M. Walkowiak, *Solid State Ionics* **2016**, *297*, 59-63.

[67] G. Salitra, E. Markevich, A. Rosenman, Y. Talyosef, D. Aurbach, A. Garsuch, *ChemElectroChem* **2014**, *1*, 1492-1496.

[68] Y-C. Lu, Q. He, H. A. Gasteiger, *J. Phys. Chem. C* **2014**, *118*, 5733–5741.

[69] D. Zheng, X. Zhang, J. Wang, D. Qu, X. Yang, D. Qu, *J. Power Sources* **2016**, *301*, 312–316.

[70] J. Liang, Z.-H. Sun, F. Li, H.-M. Cheng, *Energy Storage Mater.* **2016**, *2*, 76–106.

[71] A. Manthiram, Y. Fu, S. H. Chung, C. Zu, Y. S. Su, *Chem. Rev.* **2014**, *114*, 11751–11787.

[72] L. Carbone, A. Esau Del Rio Castillo, J. Kumar Panda, G. Pugliese, A. Scarpellinia, F. Bonaccorso, V. Pellegrini, *ChemSusChem* **2020**, *13*, 1593–1602.

[73] M. A. Pope, I. A. Aksay, *Adv. Energy Mater*. **2015**, *5*, 1500124-1500146.